Visual Abstract

Predicting fatigue crack growth behavior of coalesced cracks using the global-local superimposed technique

Mohd Shamil Shaari
Universiti Malaysia Pahang, Malaysia
shamil@ump.edu.my, https://orcid.org/0000-0002-3721-0816

Sylvia Dennis Urai
Institut Latihan Perindustrian Kota Kinabalu, Malaysia
sylvia.urai@gmail.com

Akiyuki Takahashi
Tokyo University of Science, Japan
takahash@rs.tus.ac.jp

Mohd Akramin Mohd Romlay
Universiti Malaysia Pahang, Malaysia
akramin@ump.edu.my, https://orcid.org/0000-0002-7713-4790

ABSTRACT. The S-version Finite Element Method (FEM) is known as a global-local superimposed approach that consists of two separate meshes referred to as global and local cracks. The relationship between the energy release rate and the Stress Intensity Factor (SIF) is evaluated to characterize the growth behavior of the fatigue cracks. The SIF is determined using the Virtual Crack Closure Method (VCCM). The cracks propagated in the direction of the loading before coalescing into a single crack. Each crack begins with a length of 10mm and a depth of 3mm. After the crack coalesces, the diameter of the surface crack before it breaks is 28mm, whereas the depth of the crack is 5.3mm. The V-shaped surface crack forms quickly after coalescence occurs and continues to propagate into a massive semi-elliptical surface crack before finally breaking. The result was validated and compared between S-version FEM and the analytical solution. The behavior of the fatigue crack growth shows a good agreement between both methods with small errors. The result indicates that the Root Mean Square Error (RMSE) values before coalescing are 0.1496 with 0.6, and after coalescing is 0.4, the RMSE value is 0.1665. Therefore, it can be stated that the S-version FEM approach can predict the growth of fatigue cracks.

KEYWORDS. S-version FEM; Coalesced cracks; Fatigue crack growth behaviour.

OPEN ACCESS

Citation: Shaari, M. S., Urai, S. D., Takahashi, A., Romlay, M. A. M., Predicting fatigue crack growth behavior of coalesced cracks using the global-local superimposed technique , Frattura ed Integrità Strutturale, 61 (2022) 150-167.

Received: 31.03.2022
Accepted: 10.06.2022
Online first: 21.08.2022
Published: 01.10.2022

INTRODUCTION

Fatigue fracture prediction was a critical technology when it came to ensuring the structure's integrity. Flaws or defects such as cracks greatly affect the mechanical behavior and also the performance of the structure and components themselves. The fatigue failure mostly occurs as the cyclic loading lowers that yield strength [1]. Various research and studies were previously conducted to predict fatigue failure since it impacts human safety, the economy, and the environment [2]. Fatigue crack growth occurs in complex structures, hence providing difficulties to perform the prediction [3,4]. The fatigue crack development can be caused by residual stress and the stress ratio effect, and a driving force model is used to calculate the FCG [5]. The fatigue life can be predicted by using the "small crack theory" with different materials and loading conditions [6]. Therefore, when the crack propagates at its maximum, the fracture of the material will happen. Aerospace structure and pressure vessel components possess the risk of failure towards their structural integrity. This is important to prevent any catastrophic incidents [7]. However, fatigue crack growth is difficult to predict using assumption or experience due to numerous parameters such as loading type, environment, and crack initiation location. In addition, the cracks are not necessarily formed on the surface as they might initiate and propagate inside the materials [8,9]. Nondestructive testing (NDT) is a technique that is frequently used to determine the structural integrity of oil and gas infrastructures. Other techniques, such as tomography, are usually used to examine the growth of the cracks with various materials and structures. However, these two methods were relatively expensive due to the cost of specimen preparation. Consequently, the research switched to numerical computation, which is economical and cost-effective.

The previous four decades have seen the development of numerical computation. This occurred as researchers began to comprehend the value of the Finite Element Method (FEM) as it provides faster yet economical against the experimental method. As a result, engineers can assess and validate their designs without conducting laboratory testing. Nowadays, FEM is widely utilized in structural engineering, oil and gas, aerospace, and nuclear power plant development [10,11]. The FEM process, also known as adaptive remeshing procedures, has proven to be extremely effective and dependable. However, when a fracture propagates, this method takes a long time to generate a new mesh [12]. Over the last few decades, numerous improvements to the conventional FEM have been implemented to enhance accuracy and increase its application in diverse engineering fields. One example is the introduction of S-version FEM, which is mainly applied in the fatigue and fracture mechanics field [13].

The introduction of the global-local superimposed techniques is the methodology's primary highlight. Thus, the meshes were differentiated by global mesh for the structure and local mesh for the cracks or flaws to improve the computational efficiency of the conventional FEM. The computational process was able to be simplified since the global mesh was not being included in the re-meshing process. Therefore, calculating the rate of energy release rate (G) requires less processing effort for every step of each crack propagation. Following the G formulation, the Stress Intensity Factor (SIF) can be determined concurrently with the growth of the local mesh. The SIF (K) is primarily used to anticipate the growth of cracks by calculating the stress level at the crack font by applying the virtual crack closure method (VCCM) [14]. Nevertheless, numerous investigations in the study field, particularly in the S-version FEM approach, have concentrated on a single crack. [15]. Thus, this paper will discuss the fatigue crack growth behavior of coalesced cracks using S-version FEM. The following section will describe the process for simulating crack growth using the S-version FEM.

CONCEPTS TO THE FORMULATION OF S-VERSION FEM

The concept of the S-version Finite Element Method (FEM) is illustrated in Fig. 1. The S-version FEM is used in this study to stimulate surface cracks and generate a coalesced crack under tension loading. It can be referred to as superposition mesh or superimposed mesh, which comprises a global mesh (coarser mesh) and a local mesh (finer mesh). Additionally, to reduce computing time without influencing accuracy, a global mesh and local mesh are superimposed on each other. Before being superimposed by the local mesh, Ω^L the global mesh Ω^G is generated according to geometry. The local mesh is used to illustrate the corresponding shapes and sizes of the cracks. The semi-elliptical cracks were analyzed to substantiate the results of Newman & Raju's (1979) findings in this study, with further details provided in the next section. Each region's boundaries are represented by Γ, whereby the superimposed boundary is represented by Γ^{GL}, while the displacement and force (traction) are represented by Γ^u, and Γ^t, respectively.

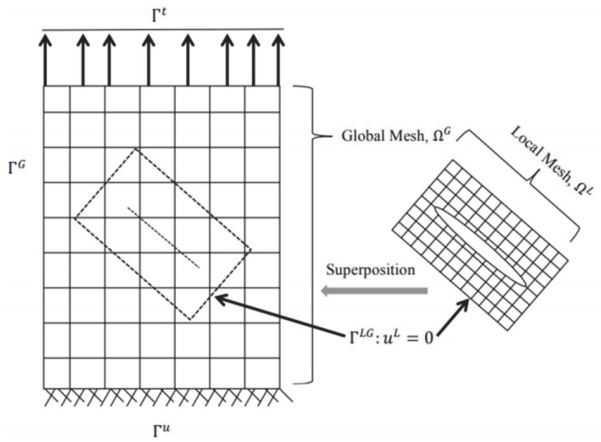

Figure 1: FEM concept in the Superimposed.

After that, the FEM concept based on the S-version is now ready for analysis. Each region (global and local), as well as the displacement function, are determined independently. When the element is loaded, both the local and global mesh displacement functions s are presumed to be independent of $u_i^G(x)$, respectively. Any displacement in the local region is the summation of the displacement for both the global and local elements. This displacement is significant since it affects the crack's growth. The function $u_i(x)$ is now given as follows:

$$u_i(x) = \begin{cases} u_i^G(x) & x \in G^\Omega - G^L \\ u_i^G(x) + u_i^L(x) & x \in G^L \end{cases} \tag{1}$$

When there is a change in nodal displacement, all potential displacements are considered. The formula is shown in Eqn. 2:

$$u_i(x) = \begin{cases} \delta u_i^G(x) & x \in G^\Omega - G^L \\ \delta u_i^G(x) + \delta u_i^L(x) & x \in G^L \end{cases} \tag{2}$$

For continuity of displacement, the displacement of the outer boundary of the local mesh $\left(\Gamma^G\right)_t$ is set to zero and variation δu_i. When it is virtually displaced, the work done by the displacing force is zero according to the principle of virtual works. By applying the virtual works principle, Eqns. 1 and 2 are set as input in the equation of virtual works equation to produce Eqn. 3 as follows:

$$\int_{\Omega^G} \delta u_{i,j} E_{ijkl} u_{k,l} d\Omega = \int_{\left(\Gamma^G\right)_t} \delta u_{i,j} t_i d\Gamma + \int_{\Gamma^{crack}} \delta u_i t_i^{crack} d\Gamma + \int_{\Omega^G} \delta u_i b_i d\Omega \tag{3}$$

The above equation accounts for virtual displacement where t_i and b_i represent the traction applied at the boundary and the force per unit volume in the element, respectively. The amount of traction force at the crack face is represented by t^{crack}. The boundary condition for both crack faces is denoted as Γ^{crack}. The boundary condition of the global element where the traction force, t_i is also present is represented by $\left(\Gamma^G\right)_t$. The second and third integral terms in Eqn. 3 are for the crack face and body force. When Eqns. 2 and 3 are placed into Eqn. 4, which is the virtual work equation, a new joint equation is formed for both global element displacement variation δu_i^G and local element displacement variation δu_i^L is drawn up in Eqns. 4 and 5 as follows.

$$\int_{\Omega^L} \delta u_{i,j}{}^G E_{ijkl} u_{k,l}{}^G d\Omega + \int_{\Omega^L} \delta u_{i,j}{}^G E_{ijkl} u_{k,l}{}^L = \int_{\left(\Gamma^G\right)_t} \delta u_i^G t_i d\Gamma + \int_{\Gamma^{crack}} \delta u_i{}^G t_i d\Gamma^{crack} + \int_{\Omega^G} \delta u_i{}^G b_i d\Omega \tag{4}$$

$$\int_{\Omega^L} \delta u_{i,j}{}^{G} E_{ijkl} u_{k,l}{}^{G} d\Omega + \int_{\Omega^L} \delta u_{i,j}{}^{G} E_{ijkl} u_{k,l}{}^{L} = \int_{\left(\Gamma^G\right)_t} \delta u_i^L t_i d\Gamma + \int_{\Gamma^{crack}} \delta u_i{}^{L} t_i d\Gamma^{crack} + \int_{\Omega^G} \delta u_i{}^{L} b_i d\Omega \quad (5)$$

The input can be of any choice based on what is being computed for, and they are also not dependent on each other. Here, freedom is given for the crack to be modeled on the local mesh for analysis. If there is an equal and opposite magnitude of traction force applied at the faces of crack, the integral for crack face traction (the second term on the right side) of Eqn. 4 cancels out. The formulas derived for S-version FEM can be used along with the discrete quantities of Ω^G and Ω^L to set up a matrix as given in Eqn. 6.

$$\begin{bmatrix} K^{GG} & K^{GL} \\ K^{LG} & K^{LL} \end{bmatrix} \begin{pmatrix} u^G \\ u^L \end{pmatrix} = \begin{pmatrix} t^G \\ t^L \end{pmatrix} + \begin{pmatrix} 0 \\ t^{crack} \end{pmatrix} + \begin{pmatrix} b^G \\ b^L \end{pmatrix} \quad (6)$$

Where

$$\begin{aligned} \left[K_{GG}\right] &= \int_{\Omega^G} \left[B^G\right]^T [D] \left[B^G\right] d\Omega \\ \left[K_{GL}\right] &= \int_{\Omega^L} \left[B^G\right]^T [D] \left[B^L\right] d\Omega \\ \left[K_{LG}\right] &= \int_{\Omega^L} \left[B^L\right]^T [D] \left[B^G\right] d\Omega \\ \left[K_{LL}\right] &= \int_{\Omega^L} \left[B^L\right]^T [D] \left[B^L\right] d\Omega \\ \left\{F_G\right\} &= \int_{\Omega^G} N^G b_i d\Omega + \int_{\Gamma^G} N^G f_i d\Gamma \\ \left\{F_L\right\} &= \int_{\Omega^G} N^L b_i d\Omega + \int_{\Gamma^G} N^L f_i d\Gamma \end{aligned} \quad (7)$$

From Eqn. 6, the nodal displacements of the local and global meshes are represented by the vectors $\left\{u^L\right\}$ and $\left\{u^G\right\}$, respectively while $\left\{t^{crack}\right\}$, $\left\{t^G\right\}$ and $\left\{t^L\right\}$ are the traction force vectors from Eqns. 4 and 5. Here, $\left[K^{GG}\right]$ and $\left[K^{GL}\right]$ are taken from the left side of Eqn. 4 while $\left[K^{LL}\right]$ and $\left[K^{LG}\right]$ are from the left side of Eqn. 5. From the equation, $\left[K^{GL}\right] = \left[K^{LG}\right]$ proves that Eqn. 6 will be symmetrical. The magnitude of the vector displacement of the global and local mesh can be obtained simultaneously. A singular global matrix will be generated if the displacement field of the global and local mesh is similar, which may occur and be eliminated when discretization is carried out.

The reader will notice the matrix $\left[K_{GL}\right]$ and $\left[K_{LG}\right]$ are symmetrical and describe the superimposed area of the stiffness matrix. Where $\left[B\right]$ is the strain-displacement matrix of the element and $\left[D\right]$ indicates the material's stress-strain relationship [16]. The nodal forces for a global presence by $\left\{F^G\right\}$ and $\left\{F^L\right\}$ for local areas while, the f^i represents the nodal forces on the crack front. Eqn. 6 can be used to compute global and local displacements.

While the local mesh expands proportionately, the global mesh remains unchanged since the sole region of interest is contained within the crack front boundary. Additionally, the global mesh will not be re-meshed during the process. As a result, it accomplishes the superposition technique's objective of reducing computation time. Using the energy release rate (G) formulation, the Stress Intensity Factor (SIF) is calculated concurrently with the expansion of the local mesh. By computing the stress condition at the crack tip, the SIF is primarily utilized in fracture mechanics to forecast crack growth. Thus, to determine the SIF, the energy release rate must be computed using the virtual crack closure method (VCCM), developed by Rybicki [14] in 1977. The following equation illustrates the energy release rate formula G:

$$G = \frac{1}{2h}\left(u_{1U} + u_{1L}\right) f_1 + \left(u_{2U} + u_{2L}\right) f_2 \quad (8)$$

where

$$E^{'} = \sqrt{GE^{'}} \tag{9}$$

Based on Eqn. 9, $E^{'}$ is determined by Young Modulus, E of material, and Poisson's ratio of material shown in Eqn. 9.

$$E^{'} = \frac{E}{\left(1-\nu^{2}\right)} \tag{10}$$

Fig. 2 illustrates the VCCM in detail and the meaning of upper and lower nodal forces and displacement.

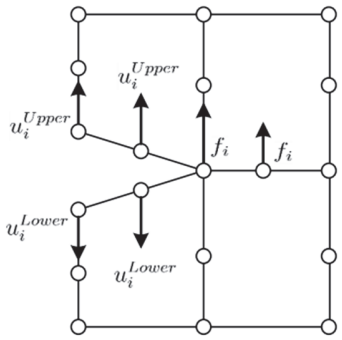

Figure 2: Illustration of calculation of the nodal displacement.

The well-known Paris law is essential for predicting the rate of fatigue fracture propagation, particularly in 2D and 3D problems. The following equation represents the Paris law:

$$\frac{da}{dN} = C\left(\Delta K_{eq}\right)^{n} \tag{11}$$

where da is the crack growth rate and N is the number of cycles. The C and n constant are depends on material properties. Therefore, it is important to consider the rate of crack formation and the direction of crack propagation, particularly in the event of mixed-mode loading. Although it is only applicable to pure mode I loading conditions in this study, the crack growth direction and equivalent stress intensity factors ΔK_{eq} should be taken into account. Moreover, Richard et al. focused on crack growth and proposed a direction criterion for crack growth. A detailed explanation can be discovered in [17]. The Richard criterion has been integrated into the software to verify that the S-version FEM is able to compute mixed-mode types of loading. Hence, this study used the equivalent stress intensity factor equation. Based on Richard's criterion, the equivalent SIF ΔK_{eq} is expressed as follows:

$$\Delta K_{eq} = \frac{\Delta K_{\mathrm{I}}}{2} + \frac{1}{2}\sqrt{\Delta K_{\mathrm{I}}^{2}} + 4\left(1.155\Delta K_{\mathrm{II}}\right)^{2} + 4\left(\Delta K_{\mathrm{III}}\right)^{2} \tag{12}$$

where ΔK_{I}, ΔK_{II}, and ΔK_{III} indicate the range of stress intensity variables associated with modes I, II, and III.

THE PROCEDURE OF CRACK GROWTH SIMULATION USING S-VERSION FEM

The approach for modeling crack growth using S-version Finite Element Method (FEM) is illustrated in Fig. 3. The entire procedure is divided into three primary stages: the development of local and global meshes, the computation of S-version FEM with the determination of crack growth rate and direction, and lastly, validation of the result using

an analytical solution based on Newman & Raju 1979 formulation. The process of simulating the crack growth is separated into several incremental steps or cycles. Therefore, the process continues until the number of maximum steps (iterations) is achieved. The S-version FEM is fully automated mesh generation, which means the local mesh will keep updating in every repetition according to both the crack propagation rate and direction. As mentioned earlier, the SIF is calculated using the VCCM. Richard's criterion is taking place to determine the crack growth direction of the crack front for the next iteration. In a nutshell, a result of SIF produced by cracks front will be used to validate the result based on the Newman & Raju equation. However, the procedure is different depending on the type of modeling and material selection. The following section exemplifies the modeling and material selection of the surface crack simulation.

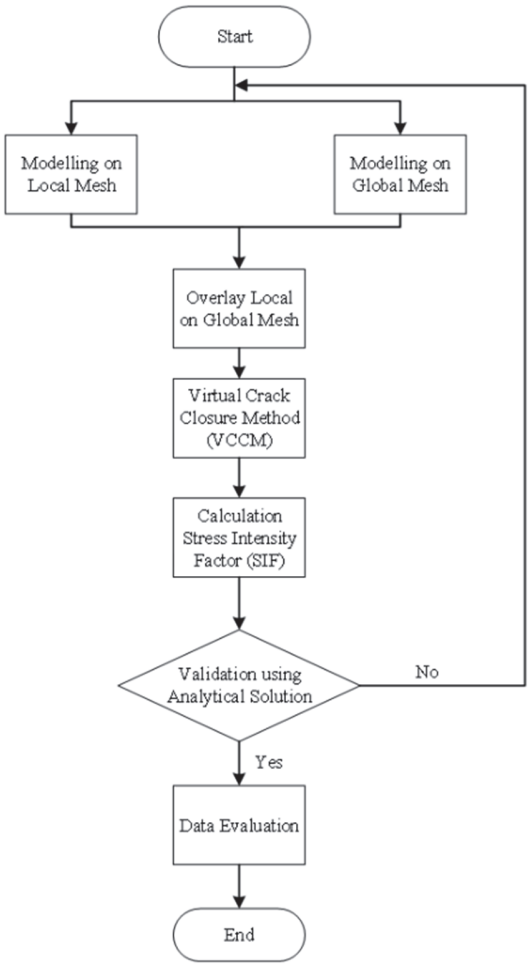

Figure 3: Procedure for crack growth simulation using S-version FEM.

MATERIAL AND MODELING SELECTION

The rectangular plate in Fig. 4 is made of A533B steel and measures 10mm by 50mm with a thickness of 100mm. The cross-section shape of the entire plate is the same, obviating the need for additional variable parameters. The rectangular plate was chosen for this study regarding the solid plate's rectangular cross-sectional geometry. The majority of cracks exemplify a closed-form solution for a finite plate. Therefore, the rectangular cross-sectional geometry, in particular, can be used to validate the numerical results. Additionally, the crack was projected to evolve into a semi-circular shape once it fully propagated. As a result, the rectangular plate is an excellent choice for the structure of this study as the crack is located in the center. In this study, the value for c is 1.67×10^{-12} and n is 3.23. Tab. 1 shows the summary of material input parameters used in this study.

No.	Material and Geometry Input Parameter	Values
1	Type of Material	A533B steel
2	Width, w	50mm
3	Thickness, t	10mm
5	Height, h	100mm
6	Load	100MPa
7	Fatigue Power Parameter, n	3.23
8	Young's Modulus, E	200GPa
9	Paris Coefficient, C	1.67 x 10^{-12} m/cycles

Table 1: Summary for material and geometry input parameter

For the fatigue testing condition, the cyclic tension loading is applied to the rectangular plate at constant amplitudes. Tension loading is commonly used for structure testing precisely to visualize large deformations. Therefore, the nature of the fatigue crack growth can be easily monitored and evaluated.

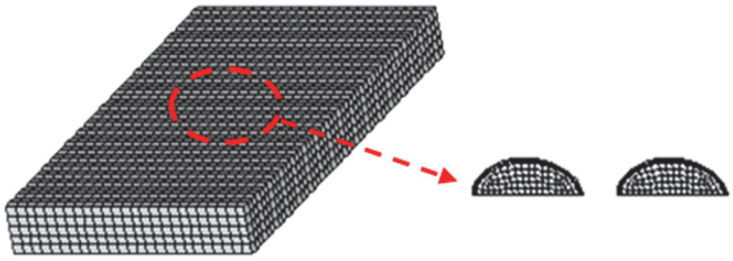

a b

Figure 4: S-version FEM (a) global mesh on the plate (b) location of the local mesh for 2 cracks.

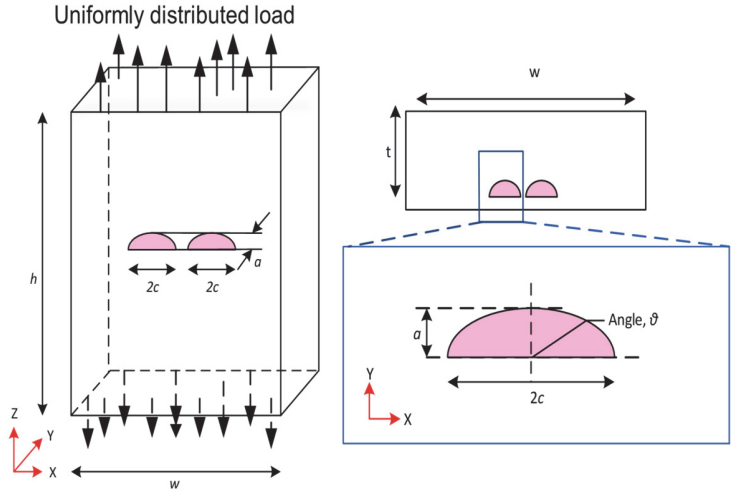

Figure 5: Location of semi-elliptical surface crack and simulation condition.

Fig. 5 shows the schematic diagram of the multiple cracks for a better understanding of the simulation's condition and location. The plate's bottom is fixed in all directions, while the top is pulled with a constant load of 100MPa. The cracks grow perpendicular to the loading axis and through the center of the rectangular plate. The crack length (c) and crack depth (a) evaluated the cracks. The result for coalescence of multiple surface crack growth will be presented and discussed next.

COALESCENCE OF MULTIPLE SURFACE CRACK GROWTH

The Stress Intensity Factor (SIF) and fracture propagation on the global-local element are stimulated. The depth and length of the crack will increase as it progresses through each stage of propagation. The surface propagation of the many surface cracks is depicted in Fig. 6, both before and during coalescence. The smaller cracks in Fig. 6 (i) indicate the original crack and grow in size proportionally to the crack propagation increments. The crack size varies according to the material used. The load applied the crack size and the shape of the crack. Starting Fig. 6 (i) until (iii) shows the two cracks propagate until both cracks are close enough to each other. When both cracks propagate, it then coalesces into a larger surface crack, as shown in Fig. 6 (iv) until (vii). The crack depth and length will grow as it progresses through each step of propagation, gradually developing towards a semi-elliptical crack.

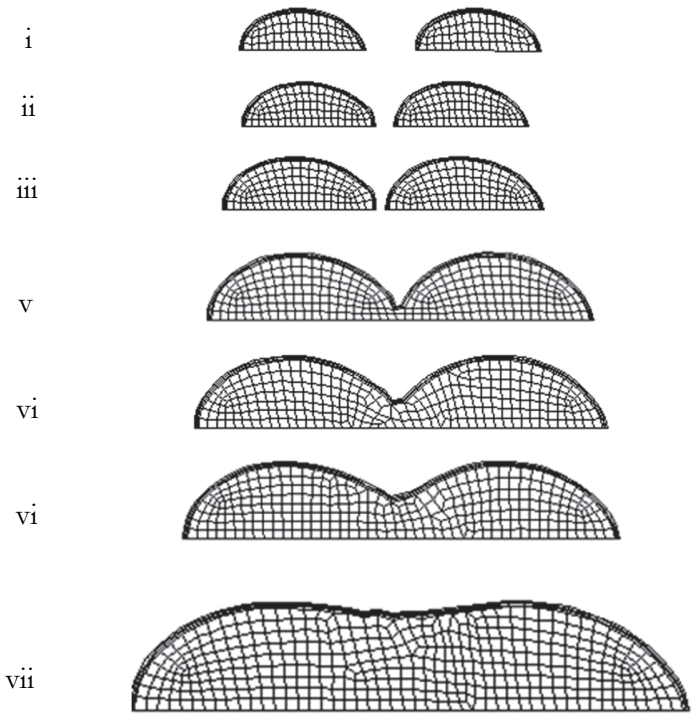

Figure 6: Surface crack propagation, before coalescence (i to iii) and after coalescence (vi to vii).

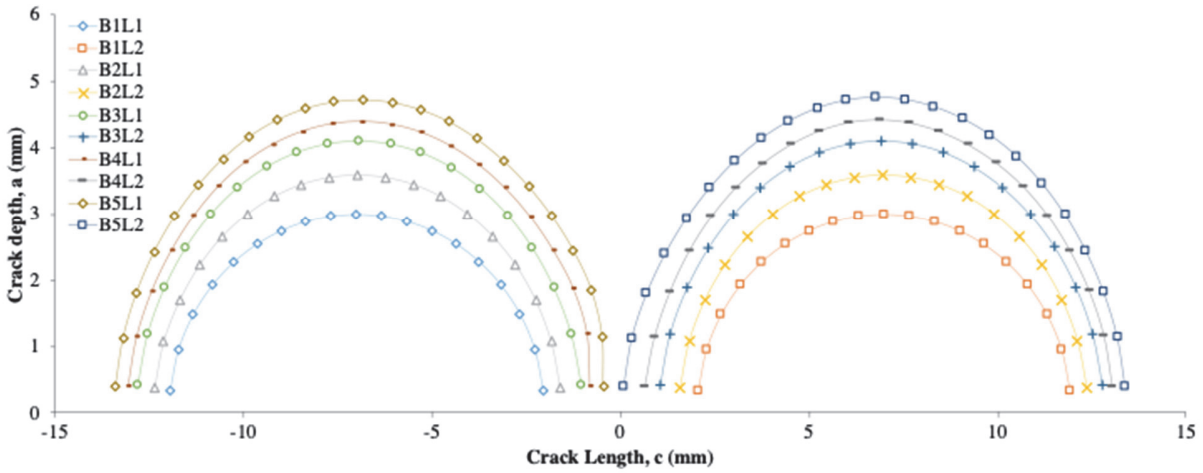

Figure 7: Crack before coalescence

Fig. 7 presents the behavior of two cracks when strain is applied to the rectangular plate based on the beach-marks (B). The propagation of the crack in the y-axis is referred to as the crack depth (a), while the crack propagation in the x-axis is referred to as the crack length (l). As for the crack length, the center of the crack is noticeably not in zero coordinate. As seen in Fig. 7, the starting dimensions of the two cracks (B1L1 and B1L2) are 10mm for the crack length (2c) and 3mm for the crack depth (a). As the fracture propagates in response to cyclic stress (B1 to B5), it is noticed that both cracks propagate gently, approximately 1mm for the 2c and 0.5mm for the a. Both fractures are on the verge of colliding, based on observations at B5. As the propagation continues, B5L1 and B5L2 consolidate into a single enormous fracture, which becomes B6.
From Fig. 8, a sharp V-shaped is formed shortly after coalescence. Still, the crack will continue to propagate into a huge semi-elliptical surface crack (B6 to B11) before the plate finally fracture. It is observed that the size of the 2c before it breaks is about 28mm and 5.3mm for the *a*. The cracking continues to grow until it achieves the limitation of the durability of the material, eventually forming a fracture. The V-shaped will form into a huge semi-elliptical. The SIF explains these events. In general, the SIF indicates crack expansion that occurs during crack propagation. The crack propagation is related to the SIF, which represents the crack propagation tendency.

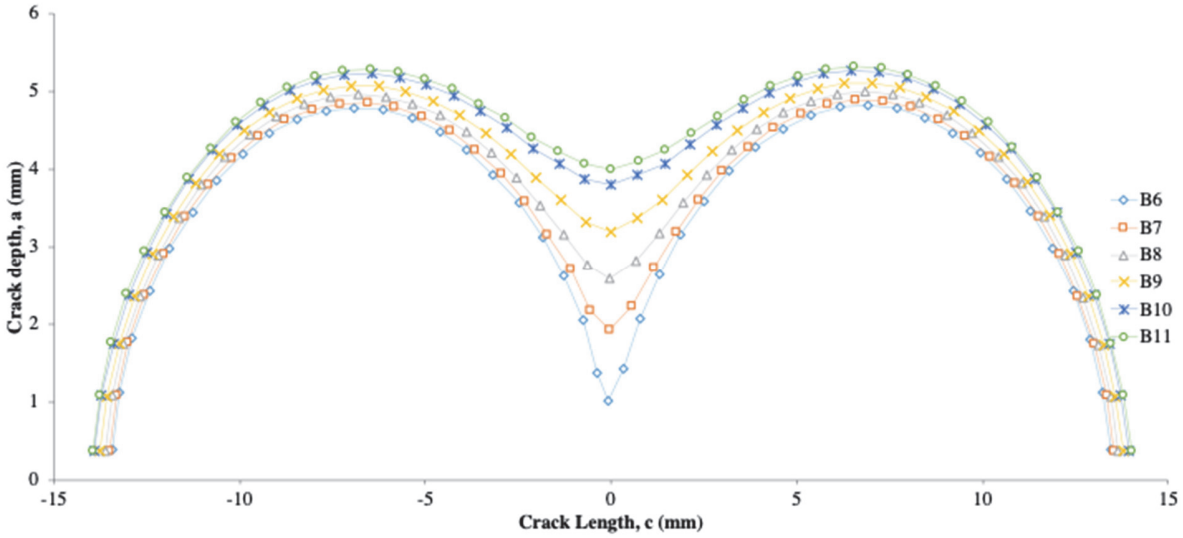

Figure 8: Crack after coalescence.

STRESS INTENSITY FACTORS EVALUATIONS

The Stress Intensity Factor (SIF) indicates the tendency of the crack propagation for an existing crack. Fig. 9 shows the behavior of the SIF for every beach-marks (B). From the figure, the x-axis represents the angle of degree (θ) for the semi-elliptical surface cracks, and the y-axis represents the SIF. First, the stress was applied uniformly uniaxially across the plate, and then the crack growth was perpendicular to the direction of tension. Thus, the semi-elliptical crack also propagates uniformly.
From the graph in Fig. 9, it is noticeable that B1 to B5 almost have a flat trend along the crack front except for B3l1 and B5L1. The lowest value for SIF before the two cracks coalesced was recorded at 8.77MPa√m for B1L1 and B1L2, whilst the highest was recorded at B3L1 at 22.30MPa√m, B5L1 at 16.49MPa√m, and B5L2 at 15.61MPa√m. This is because as the crack grows, the probability of the crack breaking into several other minor cracks is likely to occur. However, as the crack continues to propagate uniformly, the uniaxial load applied on the rectangular plate is uniformly distributed, which prevents the formation of the minor crack. Therefore, it can be observed that the crack grows smoothly between 45° and 125° along with the crack depth, unlike the crack length. This is because, at 0° and 180°, the crack face is located near to the surface but not at 90°. This is due to the sharp and tighter area near the surface. Hence, a smaller SIF value is obtained.
After the two cracks coalesced, the highest value for SIF on the crack front is at B6 at 27.60Mpa√m, followed by the second-highest value by B7 at 23.90MPa√m, B8 at 22.50MPa√m, B9 at 21.70MPa√m, B10 at 21.20MPa√m, and lastly B11 at 20.90MPa√m. It was observed that all highest SIF values were at 90°. This phenomenon is attributable to the fact that V-shaped propagated immediately after the coalescence. Therefore, the cracks are predicted to be propagated into the large

semi-elliptical surface crack. As previously stated, the SIF is correlated with the crack developing tendency. The crack propagation toward the length direction will increase proportionally with the SIF value at the crack front. The following subsection will present the validation, including verification of the S-version Finite Element Method (FEM) with an analytical solution.

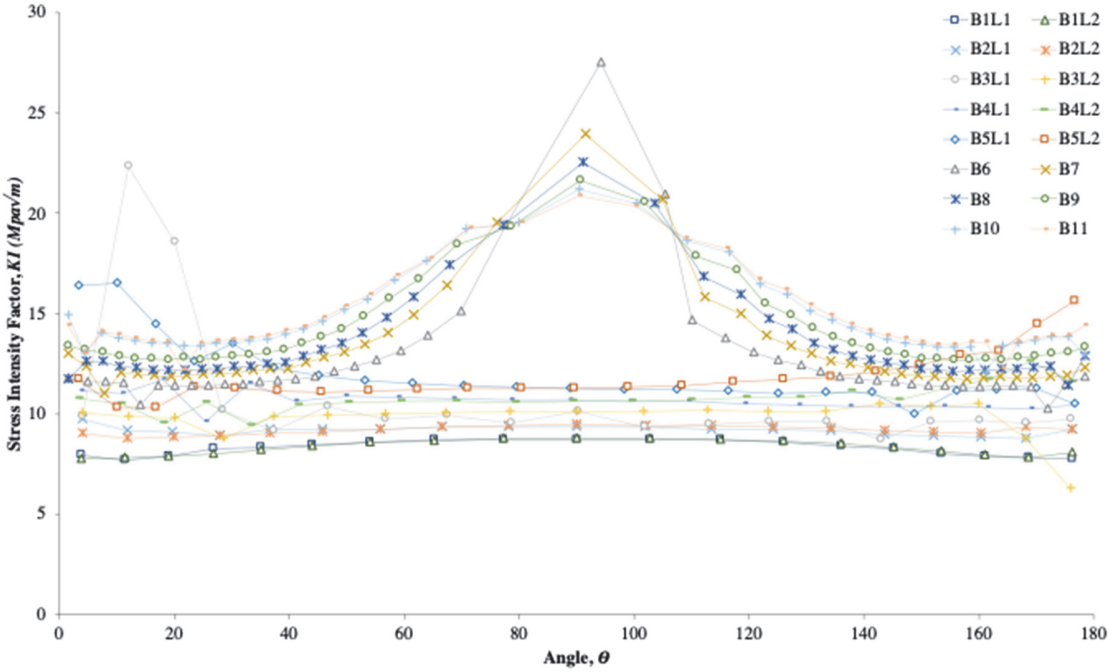

Figure 9: SIF behavior for two cracks according to the beachmarks (B) and degree of angle before and after coalesced.

VALIDATION OF S-VERSION FEM BY SIF USING THE ANALYTICAL SOLUTION

The Stress Intensity Factor (SIF) value was obtained from each beachmarks (B) is compared to the analytical solution for tension loading using the equation developed by Newman and Raju in 1979. In this study, the normalized SIF values for various B from S-version Finite Element Method (FEM) are compared to the analytical solution. From this normalized formula, $\frac{K_I}{S_t\sqrt{\pi\frac{a}{Q}}}$, the normalized SIF is computed and plotted in accordance with Newman and Raju's normalized angular direction Newman and Raju (1979).

Note that Fig. 10 (a) B1L1 and (b) B1L2 show a good agreement for both methods. The graph line of S-version FEM almost gets into one line to Newman and Raju method, indicating that Newman and Raju's method is almost similar to the result acquired of SIF using S-version FEM. Thus, to substantiate the evidence, the root means square error (RMSE) is determined. The value for the RMSE for beachmarks B1L1 and B1L2 is 0.1496.

Conversely, Figs. 11 (a) B2L1 and (b) B2L2 indicate that the line for S-version FEM is not as smooth as graph line Newman & Raju (1979) initially. However, between points 0.31 and 0.65 (normalizes angular direction), it can be observed that both graphs are in tandem, exemplifying the result of S-version FEM on that point is the same as the Newman & Raju (1979) result. The value RMSE for both beachmarks is 0.1496.

Figs. 12 (a) B3L1 and (b) B3L2 show S-version FEM is uneven to the Newman & Raju (1979) graph line initially but gradually improves to good agreement between points 0.20 to 0.80, which is in tandem for both methods. In Fig. 12 (a) it is observed that there was a spike around 0.1 normalised angular direction due to meshing errors of the crack. In contrast, the S-version FEM line at the end is decreased, as illustrated in Fig. 12 (b). However, the result for both methods still represents good agreement. The RMSE by value for both graphs is calculated to be 0.1496.

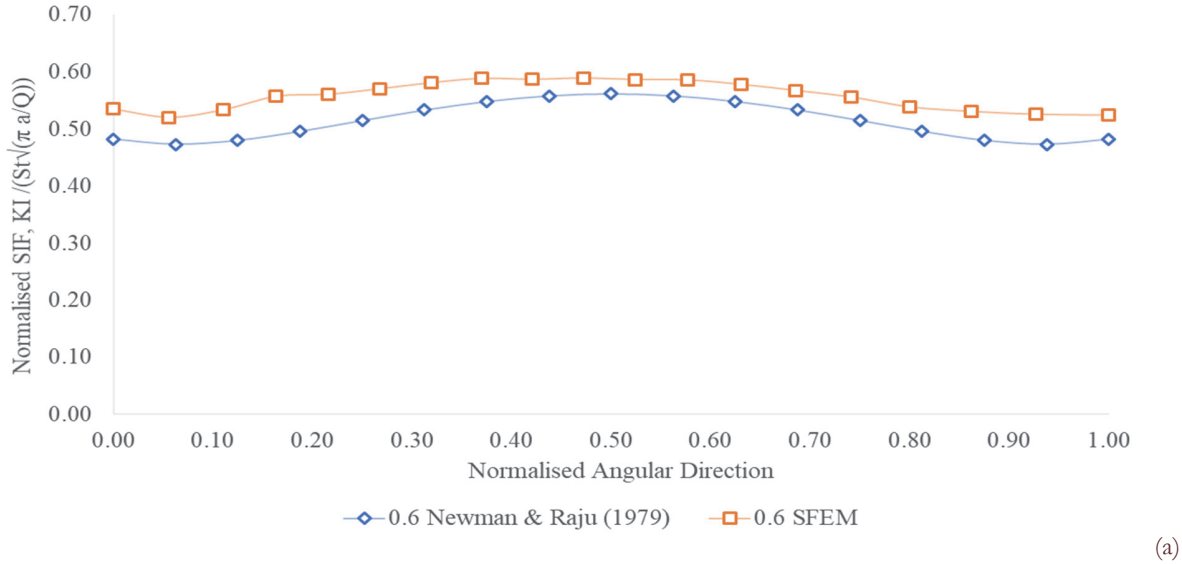

(a)

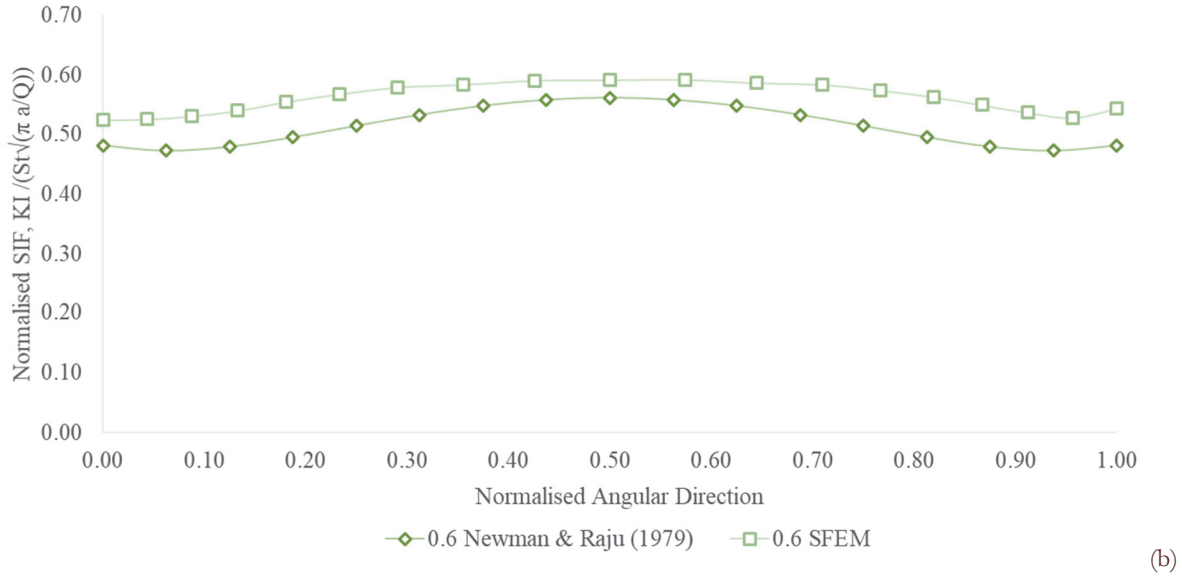

(b)

Figure 10: Normalised Stress Intensity Factor, KI corresponding with Normalised Angular Direction for (a) B1L1 and (b) B1L2

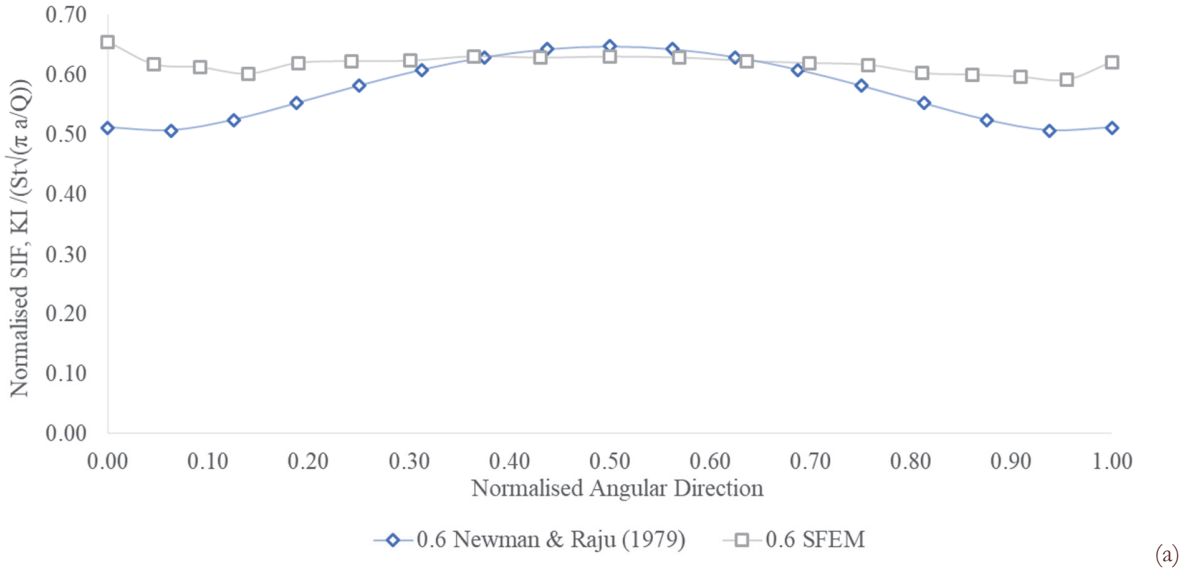

(a)

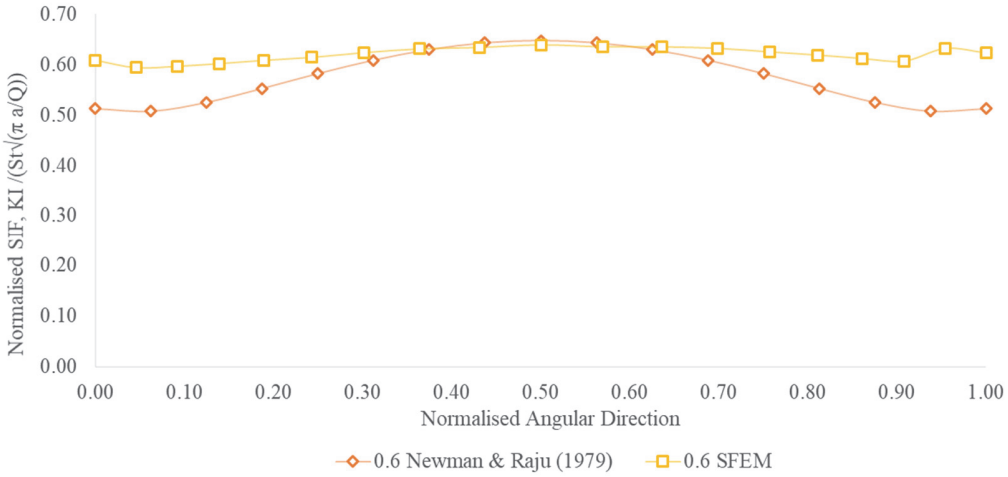

(b)

Figure 11: Normalised Stress Intensity Factor, KI corresponding with Normalised Angular Direction for (a) B2L1 and (b) B2L2

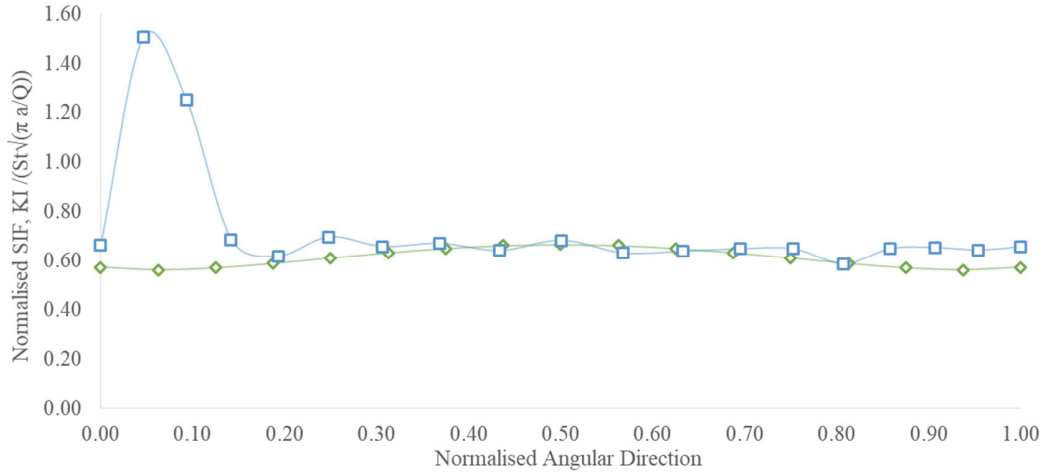

(a)

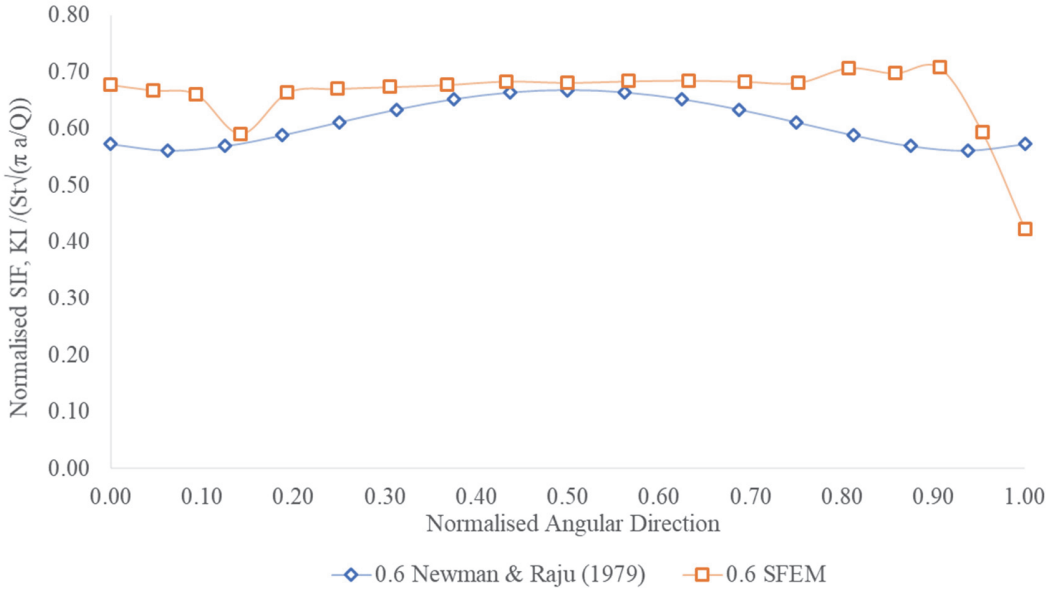

(b)

Figure 12: Normalised Stress Intensity Factor, KI corresponding with Normalised Angular Direction for (a) B3L1 and (b) B3L2

Figs. 13 (a) B4L1 and (b) B4L2 show SFEM is uneven initially. Based on Fig. 13 (a) B4L1, the line of SFEM is wavy from starting point to point 0.25. Then, the line became smooth as Newman & Raju 1979. In Fig. 13 (b) B4L2, a similar observation is made from start to point 0.25, but the end of the line increased starting at point 0.78. The cause was probably due to the re-meshing process. However, both gradually improve after point 0.22 as both methods are in good agreement, as shown in the graph. The RMSE value for both graphs is calculated to be 0.1496.

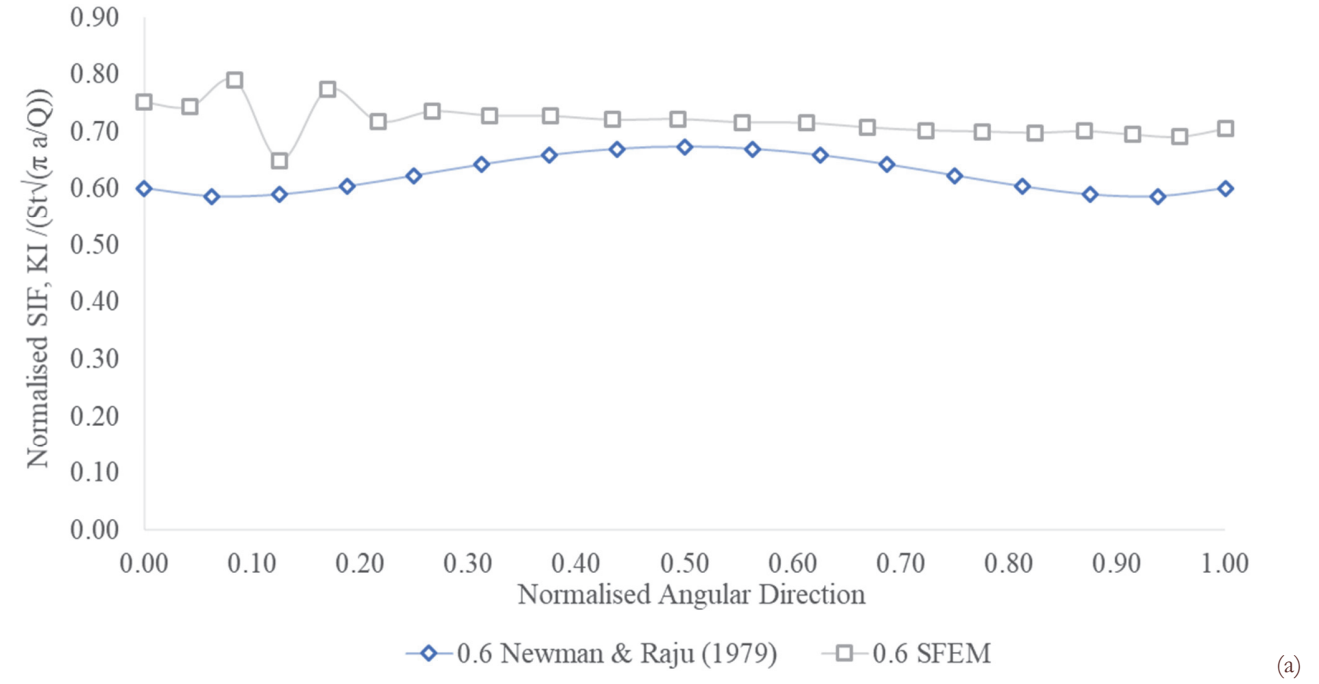

(a)

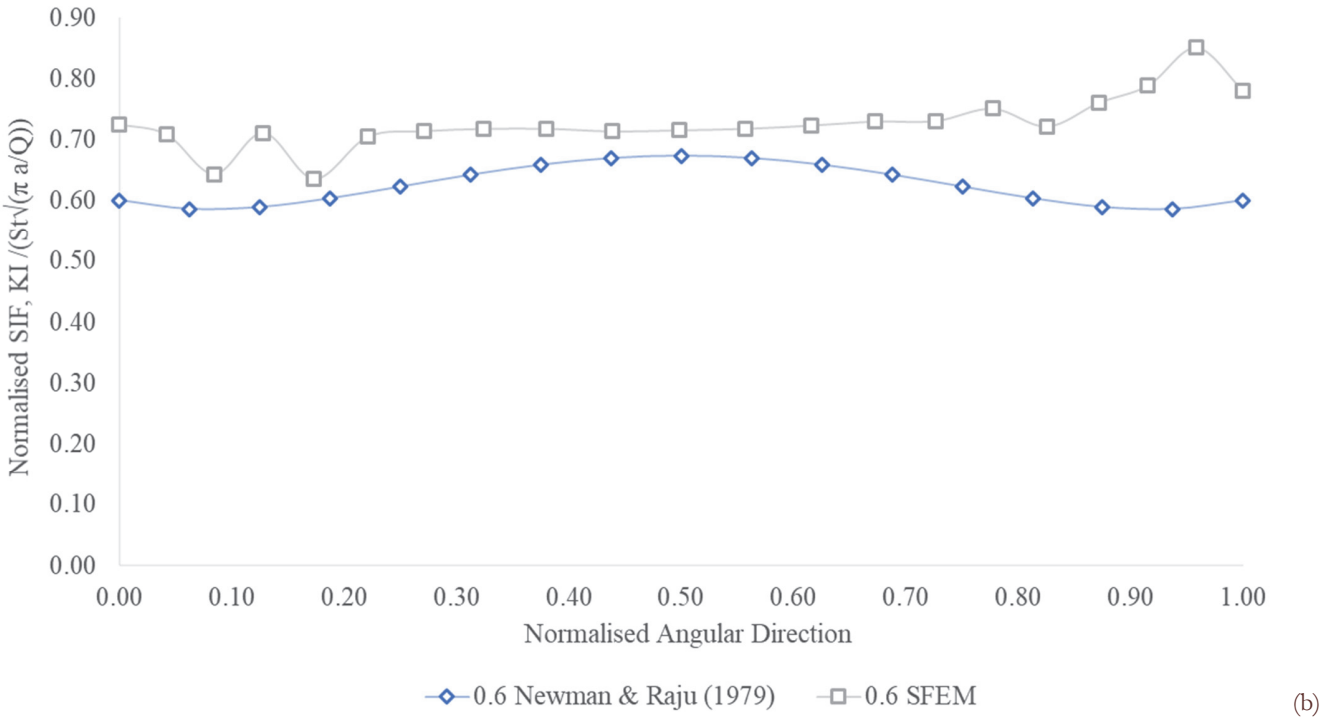

(b)

Figure 13: Normalised Stress Intensity Factor, KI corresponding with Normalised Angular Direction for (a) B4L1 and (b) B4L2

Meanwhile, the graph for SFEM is unsynchronized with the Newman & Raju 1979 graph, although both graphs represent good agreement, as illustrated by Figs. 14 (a) B5L1 and (b) B5L2. The RMSE value for both graphs is calculated to be 0.1496. It can be deducted that the limitation of the simulation and re-meshing time of the simulation contributes to the initially un-uniform line produced by the graph.

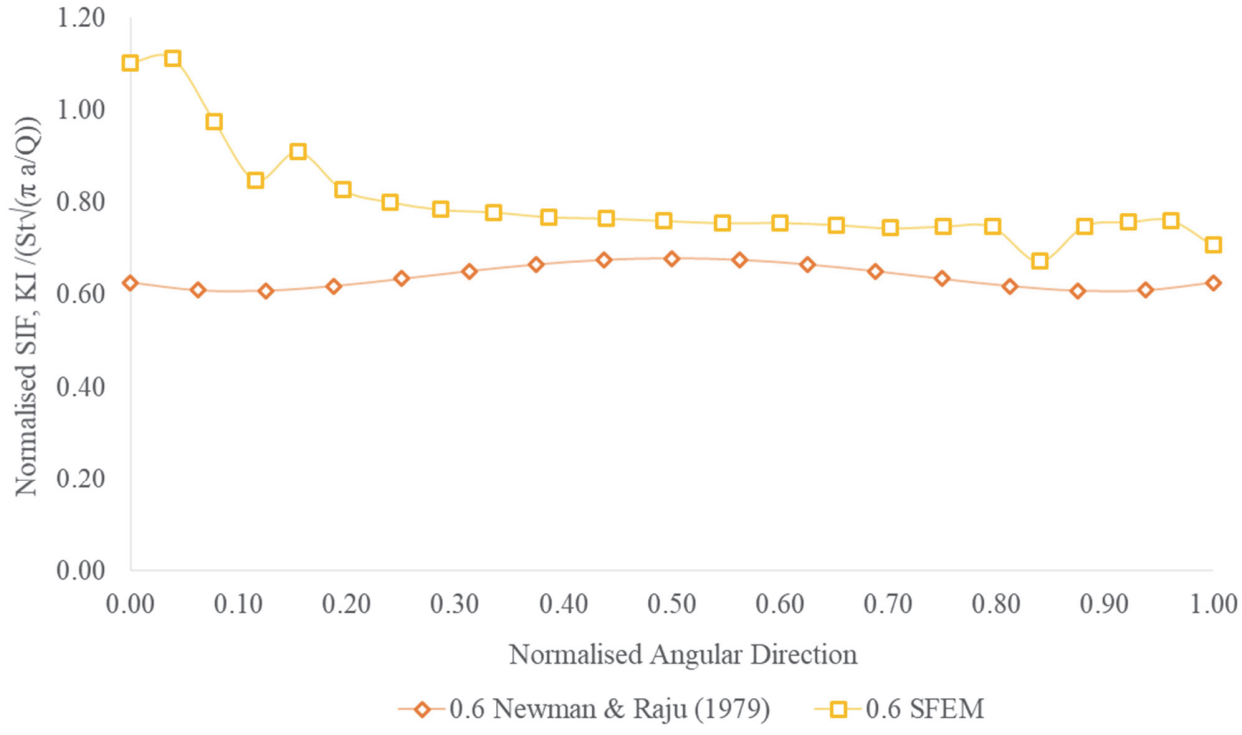

(a)

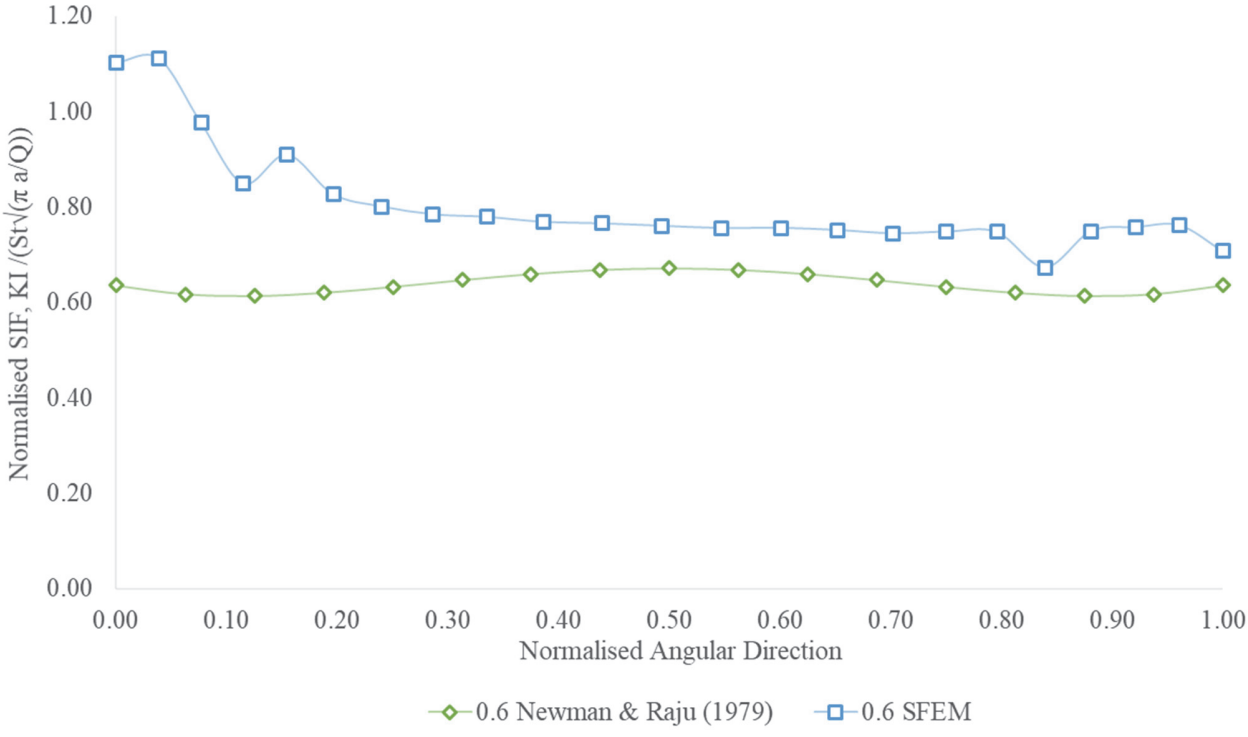

(b)

Figure 14: Normalised Stress Intensity Factor, KI corresponding with Normalised Angular Direction for (a) B5L1 and (b) B5L2

After that, Fig. 15 until Fig. 20 is validated after coalescing takes place. From Fig. 15, the point of SFEM is nearly apart from each other but at some point starting to apart. The point indicates there is a cracking process on that material. From the observation based on the graph, points 0.07 and 0.96 show the line is uneven. However, both graphs B1L1 and B1L2 show good agreement with the analytical solution. As observed, the middle part of the graph was left out as both cracks have now coalesced and the value of the SIF is at its highest point. Nonetheless, the value RMSE was evaluated at 0.1665. Fig. 16 shows the normalised SIF for B7. The starting line at the point decreases to point 0.03 but spikes at point 0.05. Still, both lines between SFEM and Newman & Raju (1979) show good agreement. The value RMSE for benchmarks from B7 is 0.1665. Fig. 17 is showing the results for B8. Based on the graph, the starting point is uneven but become smoothly rise at point 0.02 and 0.97. The point of each crack front for SFEM is close to each point but at points 0.29 and 0.73 it begins to apart. The reason is in this phase, the model starts to crack at points 0.37 and 0.62. In addition, both line still shows good agreement with the value of RMSE for beachmarks evaluated at 0.1665.

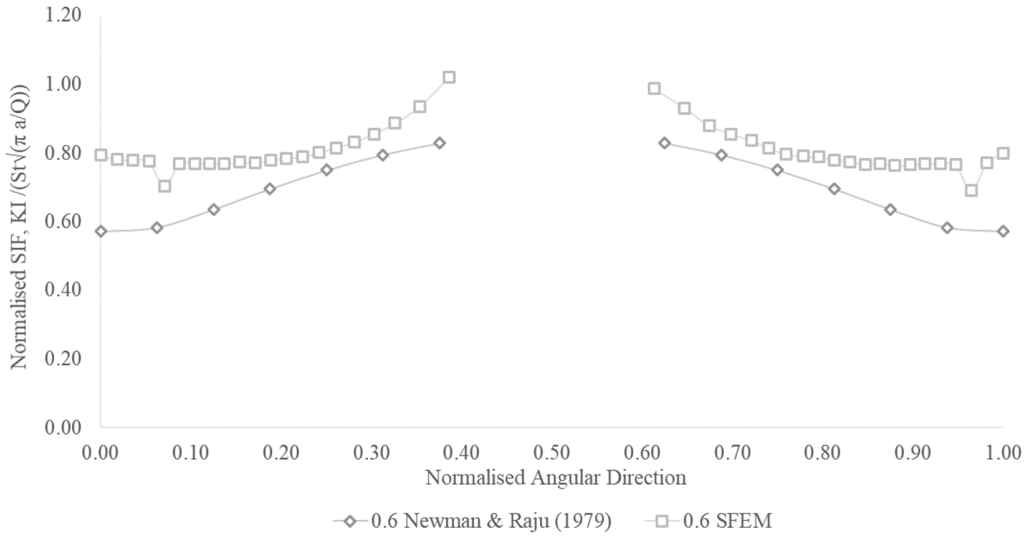

Figure 15: Normalised Stress Intensity Factor, KI corresponding with Normalised Angular Direction for B6.

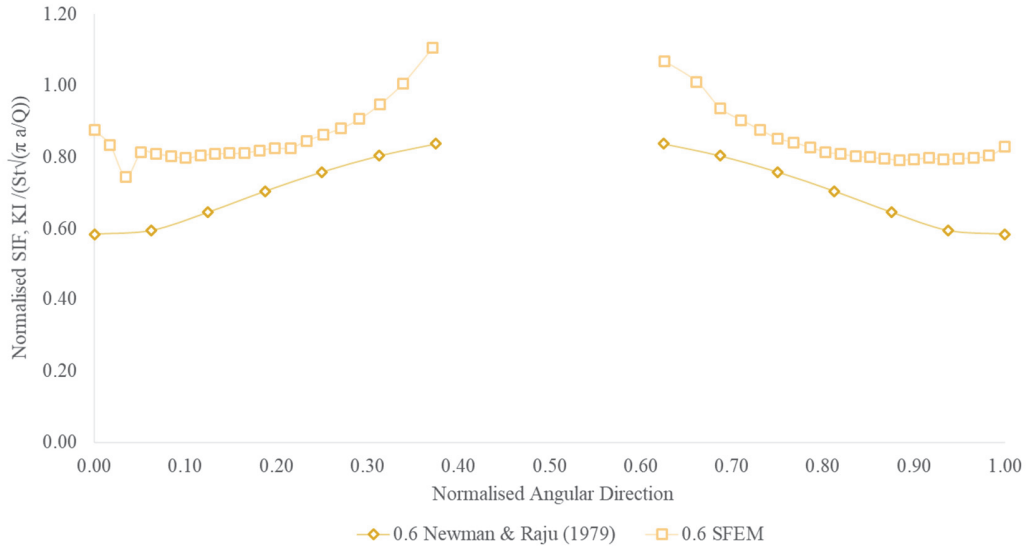

Figure 16: Normalised Stress Intensity Factor, KI corresponding with Normalised Angular Direction for B7.

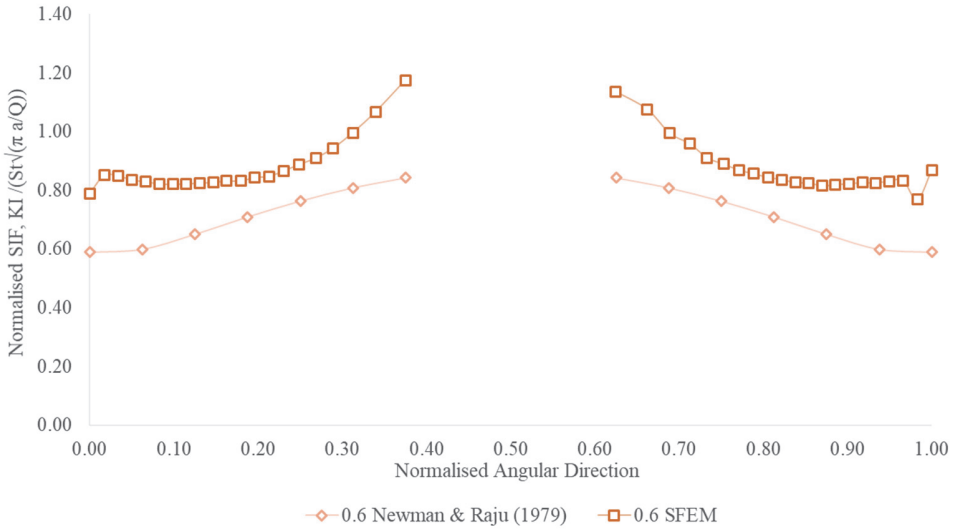

Figure 17: Normalised Stress Intensity Factor, KI corresponding with Normalised Angular Direction for B8.

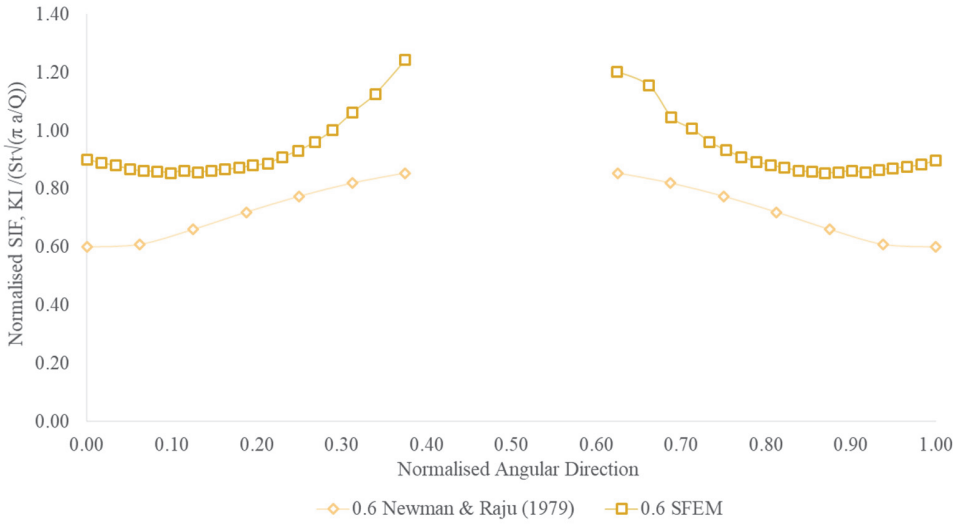

Figure 18: Normalised Stress Intensity Factor, KI corresponding with Normalised Angular Direction for B9.

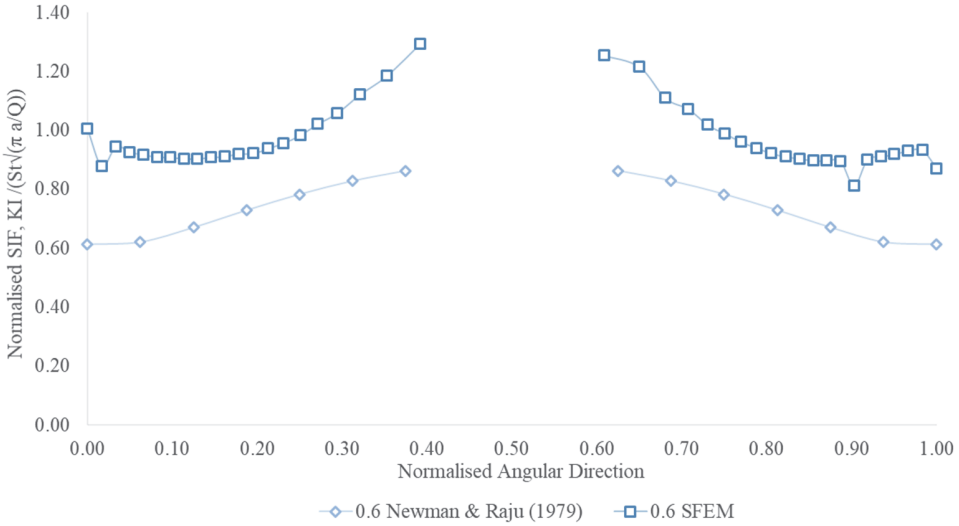

Figure 19: Normalised Stress Intensity Factor, KI corresponding with Normalised Angular Direction for B10.

The normalised SIF for B9 is presented in Fig. 18. Based on the graph, the point of each crack front for SFEM is close to each other point but at points 0.29 and 0.69 they begin to apart. The reason is in this phase, the model starts to crack at points 0.37 and 0.62, still, both line shows the good agreement between them with the value RMSE being computed at 0.1665. Then Fig. 19 it is presenting the graph for B10. Based on the graph, the starting point is uneven but become smoothly rise at point 0.03 and 0.89. The point of each crack front for SFEM seems to be close to each point but at points 0.29 and 0.68 it starts to apart. The value of RMSE for B10 is 0.1665. Finally, Fig. 20 shows observations for B11. The trend is almost similar to B10 with some fluctuations at the start and the end. Nonetheless, the value of RMSE for B11 compute at 0.1665. Even though there are some dissimilar trends and behavior for each beachmarks, the overall SIF behavior of the surface cracks still demonstrates excellent agreement between the FEM solution in the S-version and the analytical solution despite the uneven line for each graph produced.

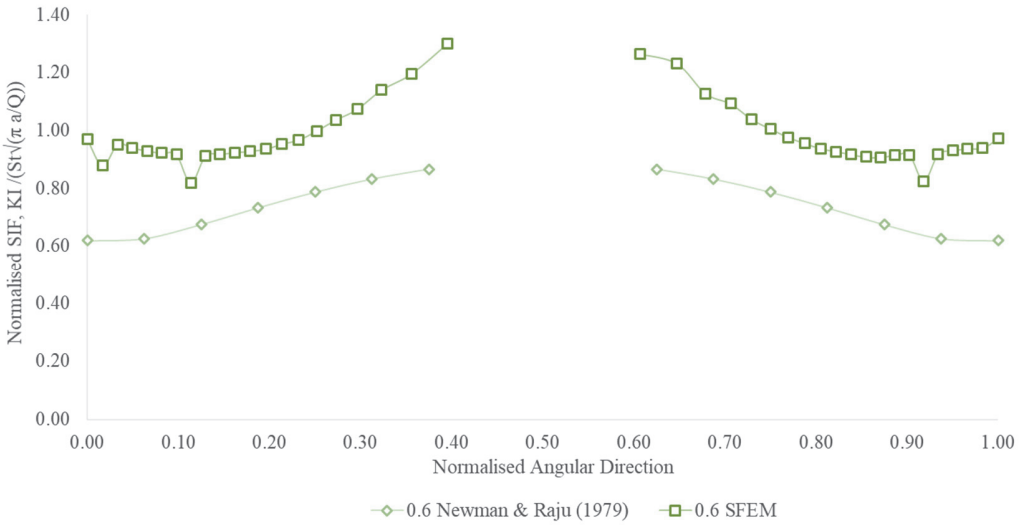

Figure 20: Normalised Stress Intensity Factor, KI corresponding with Normalised Angular Direction for B11.

CONCLUSION

The fatigue crack growth behavior of coalesced two-cracks was investigated in this study using S-version Finite Element Method (FEM). The coalescence of multiple crack growth, surface crack growth behavior, Stress Intensity Factor (SIF) evaluation, and validation of S-version FEM with the Newman & Raju equation was discussed. The conclusions are as follows:

1. The simulations successfully predicted the fatigue crack growth behavior of two cracks in a rectangular plate.
2. The initial size of the two cracks (B1L1 and B1L2) is 10mm for crack length and 3mm for crack depth. Both cracks had propagated concurrently before they coalesced into a larger surface crack. Before the rectangular plate fractured, the size of the surface crack length was observed to be at 28mm and 5.3mm for the crack depth.
3. The SIF evaluation for each beach-marks (B) was also presented. It is noticed for B1 to B5, a flat trend was observed along the crack front except for B3L1 and B5L1. The lowest value for SIF before the two cracks coalesced was recorded at 8.77 Mpa√m for B1L1 and B1L2, whilst the highest was recorded at B3L1 (22.30 Mpa√m), B5L1 (16.49 Mpa√m), and B5L2 (15.61 Mpa√m).
4. After the two cracks coalesced, the highest value for SIF on the crack front was recorded by B6 at 27.50 Mpa√m. It is then followed by the second-highest value by B7 (23.90 Mpa√m), B8 (22.50 Mpa√m), B9 (21.70 Mpa√m), B10 (21.20 Mpa√m), and B11 (20.90 Mpa√m).
5. Before the crack coalesces, the SFEM with the line NR graph shows a good agreement even at certain B, such as B3L1, B3L2, B4L1, B4L2, and B5L1. The value RMSE is calculated for each B are same as 0.1496. After the crack coalesces, the graph from B6 until B11 shows the same line as NR. The value of root means square error (RMSE) is calculated to be 0.1665.

Further studies on analytical or experimental need to be performed to validate the S-version FEM results.

ACKNOWLEDGMENT

The author would like to acknowledge the Ministry of Higher Education under Fundamental Research Grant Scheme FRGS/1/2019/TK03/UMP/02/21 (university reference RDU1901151) and Universiti Malaysia Pahang (UMP) for financial support. Also, the authors would like to thank UMP for allowing the research to be conducted using High-Performance Computer (HPC).

REFERENCES

[1] Jiang, S., Gu, Y., Fan, C.M., Qu, W. (2021). Fracture mechanics analysis of bimaterial interface cracks using the generalized finite difference method, Theor. Appl. Fract. Mech., 113, pp. 102942, DOI: 10.1016/j.tafmec.2021.102942.

[2] Azri, M.A., Shaari, S., Kamal Ariffin, A., Abdullah, S. (2018). Microstructure, Mechanical Properties and Fatigue Behavior of AlSi10Mg: an Additive Manufacturing Material, Int. J. Eng. Technol., 7, pp. 186–190.

[3] Kikuchi, M., Wada, Y., Li, Y. (2016). Crack growth simulation in heterogeneous material by S-FEM and comparison with experiments, Eng. Fract. Mech., 167, pp. 239–247, DOI: 10.1016/j.engfracmech.2016.03.038.

[4] Alshoaibi, A.M., Ali Fageehi, Y. (2022). 3D modelling of fatigue crack growth and life predictions using ANSYS, Ain Shams Eng. J., 13(4), pp. 101636, DOI: 10.1016/j.asej.2021.11.005.

[5] Kahlin, M., Ansell, H., Moverare, J. (2022). Fatigue crack growth for through and part-through cracks in additively manufactured Ti6Al4V, Int. J. Fatigue, 155, pp. 106608, DOI: 10.1016/j.ijfatigue.2021.106608.

[6] Newman, J.C., Ramakrishnan, R. (2016). Fatigue and crack-growth analyses of riveted lap-joints in a retired aircraft, Int. J. Fatigue, 82, pp. 342–349, DOI: 10.1016/j.ijfatigue.2015.04.010.

[7] Wang, Y., Shao, Y., Chen, J., Liang, H. (2021). Accurate and efficient hydrodynamic analysis of structures with sharp edges by the Extended Finite Element Method (XFEM): 2D studies, Appl. Ocean Res., 117, pp. 102893, DOI: 10.1016/j.apor.2021.102893.

[8] Cai, C., Geng, H., Cui, Q., Wang, S., Zhang, Z. (2018). Low cycle fatigue behavior of AlSi10Mg(Cu) alloy at high temperature, Mater. Charact., 145(September), pp. 594–605, DOI: 10.1016/j.matchar.2018.09.023.

[9] Alshoaibi, A.M. (2021). Computational simulation of 3D fatigue crack growth under mixed-mode loading, Appl. Sci., 11(13), DOI: 10.3390/app11135953.

[10] Shlyannikov, V., Yarullin, R., Yakovlev, M., Giannella, V., Citarella, R. (2021). Mixed-mode crack growth simulation in aviation engine compressor disk, Eng. Fract. Mech., 246, pp. 107617, DOI10.1016/j.engfracmech.2021.107617.

[11] Alves, D.N.L., Almeida, J.G., Rodrigues, M.C. (2020). Experimental and numerical investigation of crack growth behavior in a dissimilar welded joint, Theor. Appl. Fract. Mech., 109, pp. 102697, DOI: 10.1016/j.tafmec.2020.102697.

[12] Nguyen, K.D., Thanh, C. Le., Vogel, F., Nguyen-Xuan, H., Abdel-Wahab, M. (2022). Crack propagation in quasi-brittle materials by fourth-order phase-field cohesive zone model, Theor. Appl. Fract. Mech., 118, pp. 103236, DOI: 10.1016/j.tafmec.2021.103236.

[13] Fish, J. (1992). The S-version of the finite element method, 33(August 1990), pp. 1081–1105.

[14] Rybicki, E.F., Kanninen, M.F. (1977). A finite element calculation of stress intensity factors by a modified crack closure integral, Eng. Fract. Mech., 9(4), pp. 931–938, DOI: 10.1016/0013-7944(77)90013-3.

[15] Cheng, Z., Wang, H. (2019). An exact and efficient X-FEM-based reanalysis algorithm for quasi-static crack propagation, Appl. Math. Model., 72, pp. 601–622, DOI: 10.1016/j.apm.2019.02.046.

[16] Kikuchi, M. (2016). Study on multiple surface crack growth and coalescence behaviors, AIMS Mater. Sci., 3(4), pp. 1623–1631, DOI: 10.3934/matersci.2016.4.1623.

[17] Richard, H.A., Fulland, M., Sander, M. (2005). Theoretical crack path prediction, Fatigue Fract. Eng. Mater. Struct., 28(1–2), pp. 3–12, DOI: 10.1111/j.1460-2695.2004.00855.x.